ADVANCED ENERGY MATERIALS
www.advenergymat.de

Effect of Hole Transport Materials and Their Dopants on the Stability and Recoverability of Perovskite Solar Cells on Very Thin Substrates after 7 MeV Proton Irradiation

*Shi Tang, Stefania Peracchi, Zeljko Pastuovic, Chwenhaw Liao, Alan Xu, Jueming Bing, Jianghui Zheng, Md Arafat Mahmud, Guoliang Wang, Edward Dominic Townsend-Medlock, Gregory J. Wilson, Girish Lakhwani, Ceri Brenner, David R. McKenzie, and Anita W. Y. Ho-Baillie**

The drastic reduction in launch and manufacturing costs of space hardware has facilitated the emergence of "commercial" space. Radiation-hard organometal halide perovskite solar cells (PSCs) with low-cost and high-efficiency potentials are promising for space applications.High-efficiency PSCs are tested with different hole transport materials (HTMs) and dopants on 175µm sapphire substrates under 7MeV-proton-irradiation-tests at accumulated fluences of 10^{11}, 10^{12}, and 10^{13} protons cm^{-2}. While all cells retain >90% of their initial power conversion efficiencies (PCEs) after 10^{11} protons cm^{-2} irradiation, PSCs that have tris(pentafluorophenyl)borane (TPFB) as the HTM dopant and poly[bis(4-phenyl)(2,5,6-trimethylphenyl) amine (PTAA) or PTAA:C8BTBT (C8BTBT = 2,7-Dioctyl[1]benzothieno[3,2-b][1]benzothiophene) as the HTM are more tolerant to higher-fluence radiation than their counterparts with the lithium bis(trifluoromethanesulfonyl)imide (LiTFSI) dopant and the 2,2′,7,7′-Tetrakis[N,N-di(4-methoxyphenyl)amino]-9,9′-spirobifluorene (Spiro-OMeTAD) HTM. Radiation induces fluorine diffusion from the LiTFSI dopant toward the perovskite absorber (confirmed by depth-resolved X-ray photoelectron spectroscopy) introducing defects. Radiation-induced defects in cells with the TPFB dopant instead are different and can be "annealed out" by thermal vacuum resulting in PCE recovery. This is the first report using thermal admittance spectroscopy and deep-level transient spectroscopy for defect analyses on proton-irradiated and thermal-vacuum-recovered PSCs. The insights generated are expected to contribute to efforts in developing low-cost light-weight solar cells for space applications.

1. Introduction

Solar cells have been powering satellites within the Solar System since the beginning of space exploration.[1] There has been an increase in private investments in space exploration activities fueled by a reduction in launch cost and manufacturing cost of space hardware.[2,3] The high costs of the incumbent space solar cells based on group III–V materials have now become cost drivers for many space hardware. Organometal halide perovskite solar cells (PSCs) are becoming promising for space applications.[4–6] Compared to solar cells based on group III–V materials for space applications, perovskite have a lower manufacturing cost[7–10] and comparable[11–24] or even better[25,26] radiation tolerance. In addition, bandgaps of perovskites are tunable making them suitable for multijunction tandems with high power conversion efficiencies (PCEs). The highest efficiencies for single-junction perovskite and double junction perovskite-perovskite solar cells are now 25.7% (certified)[27] and 26.4% (certified),[28,29] respectively indicating ample room for improvement given the efficiency limits for double

S. Tang, C. Liao, J. Bing, J. Zheng, M. A. Mahmud, G. Wang, E. D. Townsend-Medlock, D. R. McKenzie, A. W. Y. Ho-Baillie
School of Physics
The University of Sydney
Sydney 2006, Australia
E-mail: anita.ho-baillie@sydney.edu.au

The ORCID identification number(s) for the author(s) of this article can be found under https://doi.org/10.1002/aenm.202300506

DOI: 10.1002/aenm.202300506

S. Tang, C. Liao, J. Bing, J. Zheng, M. A. Mahmud, G. Wang, E. D. Townsend-Medlock, G. Lakhwani, D. R. McKenzie, A. W. Y. Ho-Baillie
The University of Sydney Nano Institute (Sydney Nano)
The University of Sydney
Sydney 2006, Australia

S. Tang, G. J. Wilson
CSIRO Energy
Newcastle Energy Centre
10 Murray Dwyer Circuit, Mayfield West, NSW 2304, Australia

S. Peracchi, Z. Pastuovic, C. Brenner
Centre for Accelerator Science
Australia's Nuclear Science and Technology Organisation
Lucas Heights 2234, Australia

and triple junction tandems are 45% and 53%, respectively.[30] Global internet constellations on low earth orbits and in the vicinity[31,32] are the fastest growing market segment for space photovoltaics in the coming decade approaching gigawatt (GW) installations.[33] However, space hardware will be exposed to proton radiation on these orbits. Therefore, it is of great interest to evaluate radiation stability for PSCs.

Previous proton radiation stability studies for PSCs reported to date (Table S1, Supporting Information) can be divided into two groups. The first group involved direct irradiation of PSCs through their rear (first half of Table S1 in the Supporting Information) with 50 keV to 10 MeV protons[11,13,14,18,19,21–23] demonstrating excellent radiation hardness with minimum loss of PCEs under accumulated fluences of 10^{12} photons cm^{-2} (Table S1, Supporting Information). Recently, it has been shown that PSC with carbon rear electrode can withstand 150 keV proton irradiation with accumulated fluence of 10^{15} photons cm^{-2} with minimum (<0.07%) PCE loss.[24] This is outstanding as the proton irradiation fluence is equivalent to ≈1000 years of irradiation on the low earth orbits (LEOs).

The second group of proton radiation studies conducted by irradiating the front of PSCs are through quartz or glass superstrate (second half of Table S1 in the Supporting Information) with higher energy (20 and 68 MeV) protons.[12,15–17,20] This simulates the condition under which cells would operate in space—irradiation through a front cover.

In all of proton radiation studies reported for PSCs, ≥1 mm superstrates were used. To fully take advantage of high power to weight ratios, thin superstrates that are radiation tolerant should be considered. Polymer substrates deteriorate under radiations and atomic oxygen on LEOs.[34,35] Therefore, thin (175 µm/0.175 mm) sapphire substrates which have excellent optical transmittance and radiation tolerance[36] are chosen for this work. For the radiation stability studies, 7 MeV protons under accumulated fluences of 10^{11}, 10^{12}, and 10^{13} protons cm^{-2} were chosen to mimic proton radiation experienced for 1, 10, and 100 years on LEOs.[37,38]

It should also be noted that comparison of hole transport materials (HTMs) in terms of radiation hardness has not been conducted (Table S1, Supporting Information). Therefore, in this work, we compare three types of HTMs with two types of dopants that can easily be implemented in the commonly known n–i–p structure based on indium tin oxide (ITO)/tin oxide (SnO_2)/$Cs_{0.15}FA_{0.85}PbI_3$/HTM/Au as shown in **Figure 1**a. The three HTMs chosen were i) Poly[bis(4-phenyl) (2,5,6-trimethylphenyl) amine (PTAA);[39,40] ii) a mixture of PTAA with 2,2′,7,7′-Tetrakis[N,N-di(4-methoxyphenyl)amino]-9,9′-spirobifluorene (Spiro-OMeTAD)[41–43] coined "PTAA:Spiro" here after; and iii) a mixture of PTAA with 2,7-Dioctyl[1]benzothieno[3,2-b][1]benzothiophene[44–46] (C8BTBT) mixture coined "PTAA:C8BTBT" hereafter. PTAA:Spiro was considered instead of Spiro-OMeTAD alone due to the better thermal stability of PTAA compared to Spiro-OMeTAD.[47] C8BTBT was chosen to be mixed with PTAA because of its high hole mobility,[44,45] better energy level matching between the HTM and the perovskite absorber, and better solubility in chlorobenzene.[46] The two HTM dopants[40–43] being compared were i) tris(pentafluorophenyl)borane (TPFB) due to its high solubility in organic solvents,[48] strong doping capability and excellent thermal stability[40] and ii) lithium bis(trifluoromethanesulfonyl)imide (LiTFSI)[41–43] which has been used in the state of the art n–i–p perovskite cells. We found that Spiro-OMeTAD as an HTM and LiTFSI as a HTM dopant were less radiation resistant than PTAA or PTAA:C8BTBT as an HTM and TPFB as a dopant. In particular, F in the LiTFSI was more susceptible to radiation-induced diffusion to the perovskite surface introducing defects. This does not happen in cells that used TPFB as a dopant, and postradiation defects in these cells were of different kind as they could be "annealed out" by thermal vacuum (TV). Recovery of PCEs up to 100% was possible. This is convenient as TV will be experienced by the cells on LEO during Sun exposure. It is hoped that this first report of thermal admittance spectroscopy(TAS) and deep-level transient spectroscopy (DLTS) on proton-irradiated perovskite cells on ultra-thin sapphires comparing different types of HTM will provide insights into the future development of low-cost light-weight PSCs for space application.

2. Result and Discussion

Figure 1a shows the schematic of the n–i–p PSC for proton irradiation on (nominal) 175 µm (Figure S1, Supporting Information) sapphire superstrate while cross-sectional scanning electron microscopy (SEM) image of a typical PSC fabricated in this work is shown in Figure S2 (Supporting Information). Methyl-ammonium-free Cs-incorporated formamidinium based $Cs_{0.15}FA_{0.85}PbI_3$ is the perovskite material of choice due to better stability.[39,49]

For the fabrication of indium tin oxide (ITO) on sapphire, a buffer layer of Al_2O_3 is required to release mechanical stress[50] between the ITO layer and the sapphire substrate. Increasing the Al_2O_3 thickness improves the crystallinity of the ITO with the (400) peak (Figure S3q, Supporting Information) becoming dominant which is preferred for high transmittance and conductivity.[51] However, the optimal Al_2O_3 thickness is 40 nm. Above or below this value results in pinhole formation or film nonuniformity (Figure S3, Supporting Information) and slightly higher sheet resistance (Table S2, Supporting Information) in the overlaying ITO. Thicker Al_2O_3 (60 nm) also results in rougher ITO (Table S2, Supporting Information). In terms average

A. Xu
Nuclear Fuel Cycle
Australian Nuclear Science and Technology Organisation
Lucas Heights 2234, Australia
A. Xu
School of Materials Science and Engineering
University of New South Wales
Sydney, NSW 2052, Australia
J. Zheng, A. W. Y. Ho-Baillie
Australian Centre for Advanced Photovoltaics (ACAP)
School of Photovoltaic and Renewable Energy Engineering
University of New South Wales
Sydney 2052, Australia
G. Lakhwani
ARC Centre of Excellence in Exciton Science
School of Chemistry
University of Sydney
Sydney, NSW 2006, Australia

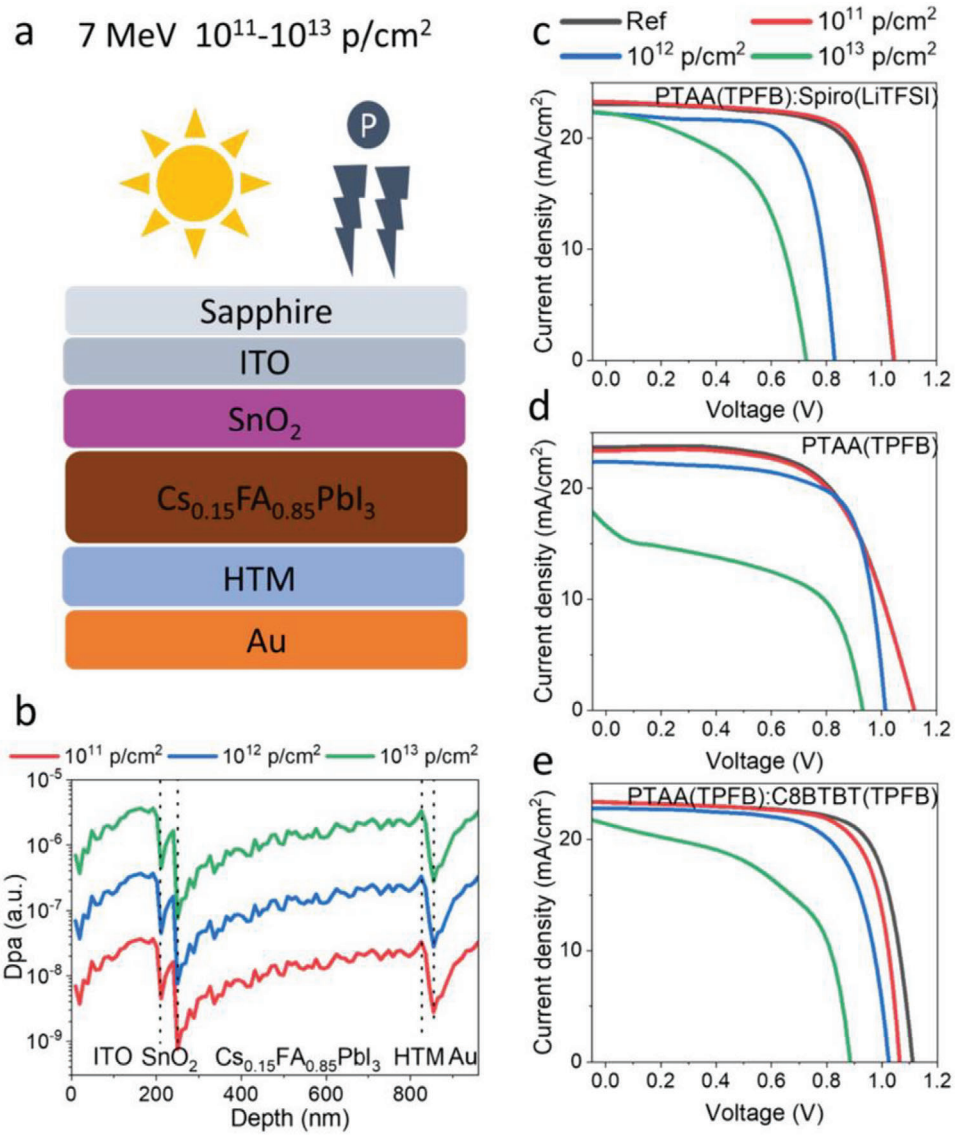

Figure 1. 7 MeV proton irradiations of PSCs. a) Schematic of cell structure and direction of proton irradiation. b) SRIM simulation of atomic displacement of the PSC with PTAA under three different proton fluences. c) *J–V* characteristics of i) PTAA(TPFB):Spiro(LiTFSI); ii) PTAA(TPFB); and iii) PTAA(TPFB):C8BTBT(TPFB) PSCs with three types of HTM before (Ref) and after irradiation with 7 MeV protons to 10^{11}, 10^{12}, or 10^{13} photons cm^{-2}.

transmittance, varying thickness of the Al_2O_3 has negligible effect (Figure S3r and Table S2, Supporting Information).

It was found that PTAA(TPFB):Spiro(LiTFSI), PTAA(TPFB) and PTAA(TPFB):C8BTBT(TPFB) based cells produced relatively higher performances. Their typical average efficiencies range from 14.9% to 17.9% resulting in very high power to weight ratios (hundreds rather than tens of mW g^{-1}) in this work compared to PSCs used in previous proton radiation studies (Table S1, Supporting Information). PTAA(TPFB):Spiro(TPFB), PTAA(LiTFSI), and PTAA(LiTFSI):C8BTBT(LiTFSI)) based cells on the other hand produced relatively lower performances (cf. Figures S6a and S7a, Supporting Information) predominantly due to lower fill factors (FFs) (cf. Figures S6e and S7e, Supporting Information) and lower output voltages (cf. Figures S6c and S7c, Supporting Information). Results suggest that the dopant TPFB is more compatible with the HTM PTAA than the dopant LiTFSI while the LiTFSI is more compatible with Spiro-OMeTAD than TPFB for high performance cells.

To determine minimum proton energy that will penetrate through the 175 μm sapphire superstrate, stopping and range of ions in matter (SRIM)[52,53] simulation was used first. Result (Figure S4, Supporting Information) shows that a proton with the threshold energy of 6.35 MeV is required. As 7 MeV protons lose their energy through the superstrate, protons with the energy of 697.39 keV were used for simulating atomic displacements through each layer in PSCs beyond the superstrate. Parameters for the simulation can be found in Table S3 (Supporting Information). Results (Figure 1b) show similar displacement trends for fluences at 10^{11}, 10^{12}, and 10^{13} protons cm^{-2} with displacement density increasing with the depth in each layer. The

boundaries conditions setup in the SRIM model assumes boundaries between layers at depth of approximately 200, 250, and 840 nm are noninteractive. Hence, displacement cascade produced in the previous layer does not propagate into the next layer. Once the hydrogen ion penetrates the new layer, the displacement cascade starts a new causing the displacement to increase with depth in the new layer. The difference in displacement between layers is also exacerbated by the inherent differences in displacement energy between atomic species of different layers.[54,55] Figure 1c–e shows the current density (J)–voltage (V) characteristics of the better performing PTAA(TPFB):Spiro(LiTFSI), PTAA(TPFB) and PTAA(TPFB):C8BTBT(TPFB) based PSCs before and after 7 MeV irradiation at three fluence levels, respectively. Details of cell packaging and proton radiation performed can be found in the Experimental Section, in Figure S5 and Table S4 (Supporting Information). Distribution of other cell parameters for the higher performing PTAA(TPFB):Spiro(LiTFSI), PTAA(TPFB) and PTAA(TPFB):C8BTBT(TPFB) based PSCs before and after radiation can be found in Figure S6a,c,e,g,i,k (Supporting Information). For the purpose of comparison, distribution for the lower performing PTAA(TPFB):Spiro(TFPB), PTAA(LiTFSI) and PTAA(LiTFSI):C8BTBT(LiTFSI) PSCs can be found in Figure S7 (Supporting Information) although the majority of the initial discussion on results and analyses in the main text will focus on the higher performing cells.

While all of the PSCs retained 90% of their initial PCEs after the fluence of 10^{11} protons cm^{-2} (Figure S8, Supporting Information), cells with C8BTBT in their HTMs are more stable than the ones without C8BTBT after the fluence of 10^{12} photons cm^{-2} and after 10^{13} photons cm^{-2} irradiation retaining around 60% of initial PCEs for the cells with C8BTBT. The biggest contributor to performance drop is the decline in FFs (Figures S6e and S7e, Supporting Information). Spiro-OMeTAD containing cells had the largest open-circuit voltage (V_{OC}) drop after 10^{12} photons cm^{-2} while cells without Spiro-OMeTAD experienced dramatic V_{OC} drop only until after 10^{13} photons cm^{-2} (Figures S6c and S7c, Supporting Information). This is not surprising as radiation-induced degradation in spiro-OMeTAD and therefore in associated solar cells has recently been previously reported.[11] Regarding short-circuit current (J_{SC}) drop (Figure S6g, Supporting Information), PTAA-only (whether LiTFSI or TPFB doped) cells suffered the most after 10^{13} photons cm^{-2} radiation while other cells experienced smaller deterioration in output currents postradiation. To ascertain whether changes in the optical properties of the sapphire superstrates occurred postirradiation, transmittance measurements were conducted before and after 10^{12} photons cm^{-2} irradiation. No changes could be observed (Figure S9, Supporting Information) suggesting J_{SC} drop if observed were due to radiation-induced-damage in cells alone. In terms of FF drop, major deterioration in the parasitic resistances (Figures S6i,k and S7i,k, Supporting Information) is the main contributor for the 10^{13} photons cm^{-2} irradiated cells. This can be seen in the PTAA(TPFB):Spiro(LiTFSI) cells where the initial low series resistance (R_S) and therefore high initial FF (and high initial PCE) advantages were lost after 10^{13} photons cm^{-2} irradiation. For cells after lower fluences of irradiation (10^{11} to 10^{12} photons cm^{-2}), contributor to FF drop was a combination of a mild deterioration in the parasitic resistances and an increase in defect density leading to increased carrier recombination.

Therefore, defect analyses using TAS and DLTS were carried out. Results for the higher performing PTAA(TPFB):Spiro(LiTFSI), PTAA(TPFB) and PTAA(TPFB):C8BTBT(TPFB) based PSCs are shown in **Figure 2** and summarized in Table S5 (Supporting Information). Cell parameters are shown in Table S6 (Supporting Information).

From the TAS (Figure 2a–c) results, three main defect energy levels E_{t1}, E_{t2}, and E_{t3} near 0.301, 0.310, and 0.321 eV from the valence band can be identified. PTAA(TPFB):Spiro(LiTFSI) cells also have an order of magnitude higher density of defect states compared to the PTAA(TPFB) and PTAA(TPFB):C8BTBT(TPFB) PSCs according to TAS. E_{t2} remained dominant before and after proton-irradiation in PTAA(TPFB):Spiro(LiTFSI) PSCs, while Et_1 and Et_3 became dominant after prolonged 10^{13} photons cm^{-2} irradiation in PTAA(TPFB) PSCs. Et_3 (deeper) defects became most dominant in PTAA(TPFB):C8BTBT(TPFB) PSCs after prolonged 10^{13} photons cm^{-2} irradiation. In terms of the least number of defects and radiation hardness, PTAA(TPFB):C8BTBT(TPFB) PSCs are the best followed by PTAA(TPFB) PSCs and then PTAA(TPFB):Spiro(LiTFSI) cells.

Similar trend can be observed in DLTS (Figure 2d–f) results, PTAA(TPFB):C8BTBT(TPFB) PSCs had the lowest defect densities (at E_V+0.43 eV (Table S6, Supporting Information)) before and after irradiation. In PTAA(TPFB) cells, E_V+0.43 eV and E_V+0.31 eV defects can be measured even before irradiation but only E_V+0.43 eV density of states increased with irradiation (Table S5, Supporting Information). Similar trends can be observed in PTAA(TPFB):Spiro(LiTFSI) cells which had the highest density of defects and in addition, E_V+0.68 eV defects started to emerge after prolonged irradiation (10^{13} photons cm^{-2}).

We then conducted temperature-dependent V_{OC} measurements on these cells to identify the dominant recombination mechanism. Results are shown in Figure S10 (Supporting Information) which also show the extrapolated activation-energies (E_A's) of recombination currents. The E_A trends for the higher performing cells are plotted in Figure 2g–i. E_A of the PTAA(TPFB):Spiro(LiTFSI) cell was the lowest to start with and dropped with irradiation to values well below the cell's bandgap (Figure S11, Supporting Information). This indicates that surface recombination dominates in these cells and is accelerated by irradiation. On the other hand, PTAA(TPFB) and PTAA(TPFB):C8BTBT(TPFB) PSCs had higher E_A's initially suggesting that bulk recombination dominated in preirradiated cells and even after mild levels of irradiation (10^{11} photons cm^{-2}). At higher levels of irradiation, surface recombination became more prominent as E_A's dropped with irradiation in these cells. Similar to trends observed on cell performance and defects, PTAA(TPFB):Spiro(LiTFSI) cells were the worst while PTAA(TPFB):C8BTBT(TPFB) were the best in terms of high values of E_A.

To understand the effect of proton irradiation on the HTM and HTM/perovskite interface, depth-resolved X-ray photoelectron spectroscopy (XPS)[56–58] was conducted on the cells with the Au electrode removed. **Figure 3**a–c shows the atomic ratios of fluorine to iodine as a function of depth toward the perovskite absorber in cells with PTAA(TPFB):Spiro(LiTFSI), PTAA(TPFB) and PTAA(TPFB):C8BTBT(TPFB), respectively. The plots were calibrated using the perovskite bulk (on the right) as reference point (characterized by Pb XPS signal at steady state (not shown)).

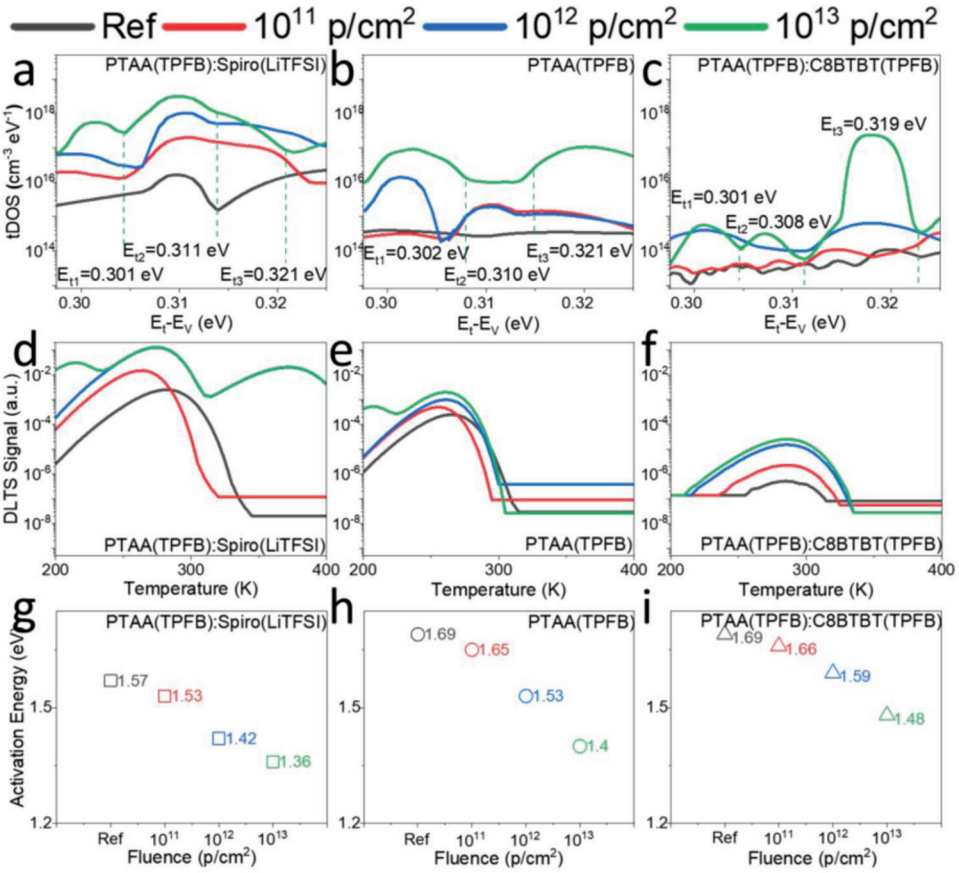

Figure 2. Defect analyses for PSCs with different hole transport materials by a–c) thermal admittance, d,f) deep level transient spectroscopies, and g–i) activation-energies (E_A) of recombination currents for cells with a,d,g) PTAA(TPFB):Spiro(LiTFSI); b,e,h) PTAA(TPFB), and c,f,i) PTAA(TPFB):C8BTBT(TPFB) before and after irradiation with 7 MeV protons to 10^{11}, 10^{12}, or 10^{13} photons cm^{-2} .

Therefore, 0 nm indicates region near the HTM/perovskite interface. For PTAA(TPFB):Spiro(LiTFSI) cells, we can already observe a wider distribution of higher fluorine to iodine ratio near the HTM/perovskite interface even before proton irradiation. The ratio peak shifts toward the perovskite bulk could be observed after 10^{12} and 10^{13} photons cm^{-2} irradiation. To ascertain the major cause for such observation, we calculated the rate of the change of the fluorine and iodine XPS signals before and after irradiation. Results in Figure S12a (Supporting Information) show greater rate of change[59] of fluorine compared to iodine suggesting fluorine diffusion into the perovskite bulk being the main culprit. PTAA(TPFB) and PTAA(TPFB):C8BTBT(TPFB) cells on the other hand had narrower distributions of fluorine to iodine ratios closer to the surface with PTAA(TPFB):C8BTBT(TPFB) cells having the narrowest distribution. Together with results from Figure S12b,c (Supporting Information), we can conclude that there is a smaller extent of fluorine (or iodine if any) interdiffusion between the HTM and the perovskite bulk postirradiation in these two types of cells. The phenomena observed helped explain the surface recombination trends observed: worst in PTAA(TPFB):Spiro(LiTFSI) cells (to begin with and postradiation which worsened with the level of radiation) and least affected in PTAA(TPFB):C8BTBT(TPFB) postirradiation compared to PTAA(TPFB) cells.

Proton induced radiation damage has been reported to be reversible for III–V space cells[60] and PSCs.[13] We therefore carried out TV treatment (a condition that can be experienced by cells in the LEOs) on proton-irradiated PSCs. Details of the TV treatment can be found in the Supporting Information. Results (Figures S6b and S7b, Supporting Information) show that PCEs of cells using LiTFSI as a HTM dopant could not recover but in fact deteriorated after TV.

Recalling previous discussion on irradiated cells, the biggest contributor to performance drop was the decline in FFs (FFs) (Figures S6e and S7e, Supporting Information) even when the cells could retain their V_{OC}'s until after 10^{13} photons cm^{-2} irradiation (Figure S6c, Supporting Information). TV treatment helped Spiro-OMeTAD-free cells and LiTFSI-free cells such as PTAA(TPFB) and PTAA(TPFB):C8BTBT(TPFB) cells to fully recover if they were exposed to lower dose ($\leq 10^{12}$ photons cm^{-2}) of irradiation or partially recover if the previous irradiation was high (e.g., 10^{13} photons cm^{-2}) (Figure S6f, Supporting Information). It is interesting to note that FF recovery is not necessarily achieved via R_S and R_{SH} recoveries (Figure S6j,l, Supporting Information) but by reduced recombination. This is confirmed by TAS, DLTS and temperature dependent V_{OC} measurements.

Results in **Figure 4**b,c,e,f and Figure S13a (Supporting Information) showed that density of defects states was

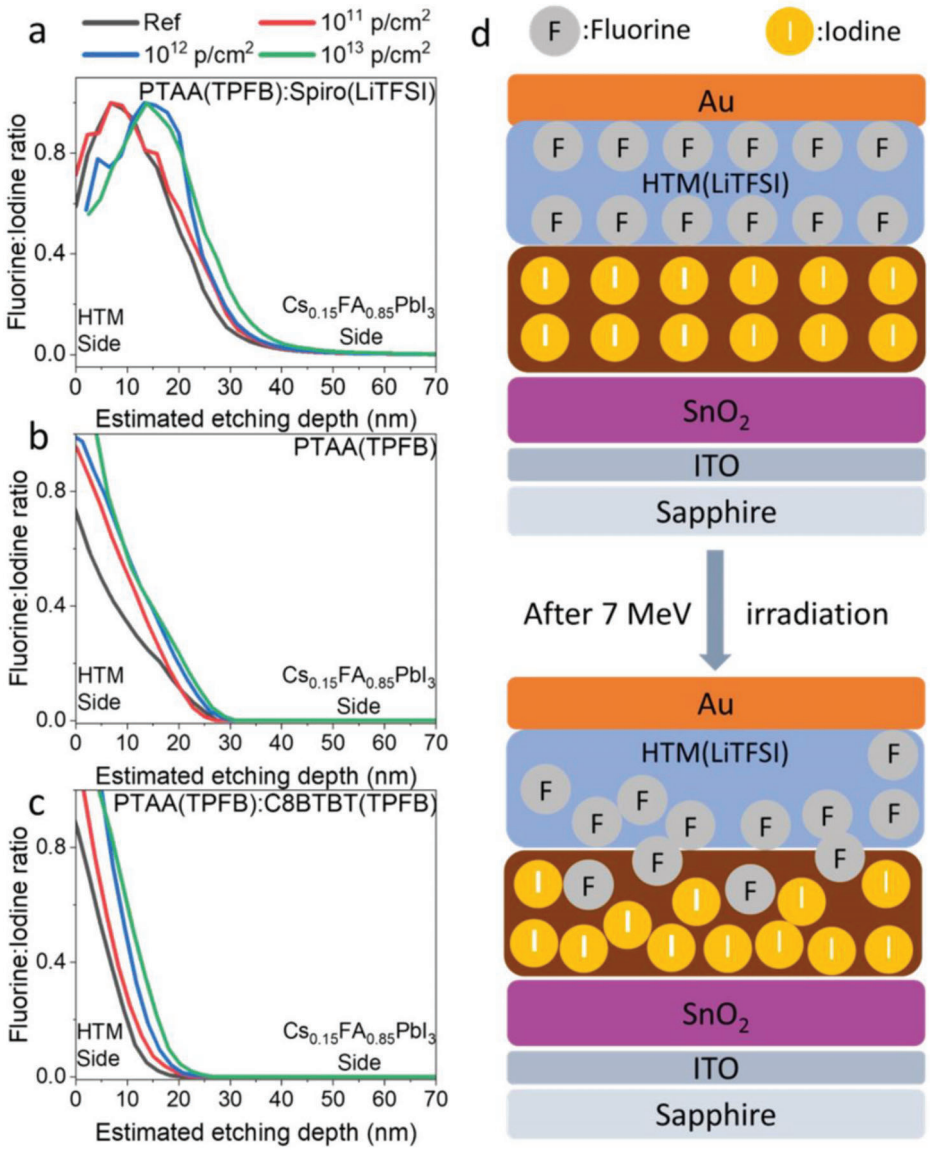

Figure 3. Chemical analysis by X-ray photoelectron spectroscopy (XPS) depth profiling of the HTM surface and HTM/perovskite interface. Atomic fluorine to iodine ratio as a function of estimated depth for a) PTAA(TPFB):Spiro(LiTFSI), b) PTAA(TPFB) c), and PTAA(TPFB):C8BTBT(TPFB) cells before and after irradiation. d) Cartoon showing F diffusion in HTM(LiTFSI) cells.

reduced post-TV treatment for LiTFSI-free cells such as PTAA(TPFB) and PTAA(TPFB):C8BTBT(TPFB) and even PTAA(TPFB):Spiro(TPFB) cells. The Et_1 and Et_3 dominance in heavily (10^{13} photons cm^{-2}) irradiated PTAA(TPFB) PSCs subsided after TV treatment (Figure 4b). The strong Et_3 peak in heavily (10^{13} photons cm^{-2}) irradiated PTAA(TPFB):C8BTBT(TPFB) cells also subsided after thermal treatment (Figure 4c).

E_A's for LiTFSI-free such as PTAA(TPFB), PTAA(TPFB):C8BTBT(TPFB) and even PTAA(TPFB):Spiro(TPFB) cells also rose back to high values after thermal treatment (Figure 4h,i; Figure S13d, Supporting Information) suggesting improvement in the cell surfaces in these thermally treated irradiated cells with bulk recombination becoming dominant. On the other hand, radiation-induced surface recombination in LiTFSI containing PSCs was irreversible and in fact became worse as E_A's dropped further after thermal treatment (Figure 4g; Figure S13e,f, Supporting Information).

This can be explained by the worsening of fluorine diffusions in thermally treated and proton-irradiated LiTFSI containing cells confirmed by depth-resolved (XPS) (Figure S14a,e,f, Supporting Information). However, the fluorine to iodine ratios in LiTFSI-free and especially Spiro-OMeTAD-free cells such as PTAA and PTAA:C8BTBT cells were not affected by thermal treatment (Figure S14b,c, Supporting Information). For the PTAA(TPFB):Spiro(TPFB) cell, small degree of fluorine or iodine diffusion might have happened (Figure S14d, Supporting Information). Nevertheless, we have successfully shown that surface recombination postradiation (not caused by fluorine diffusion) in LiTFSI-free cells can be "annealed out" by thermal treatment.

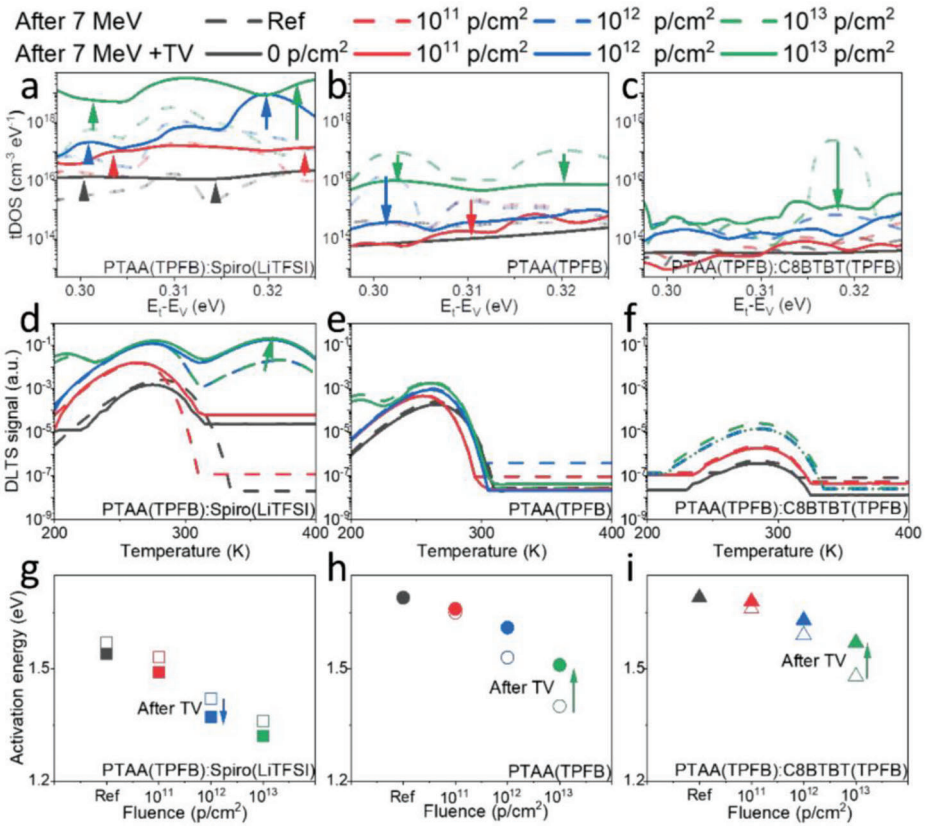

Figure 4. Effect of thermal-vacuum annealing on proton-irradiated perovskite solar cells. a–c) thermal admittance spectroscopy, d–f) deep level transient spectroscopy and g–i) activation-energies E_A's proton-irradiated a,d,g) PTAA(TPFB):Spiro(LiTFSI), b,e,h) PTAA(TPFB), and c,f,i) PTAA(TPFB):C8BTBT(TPFB) perovskite solar cells before and after post-thermal (80 °C for 30 min) vacuum treatment.

As part of the supplementary experiment requested during the reviewing process, 10 and 1 MeV proton irradiations were also conducted on representative cells to verify calculations in Figure S4 (Supporting Information).

As expected, radiation damage (cf. Figure S15a,b and Figure S6a,b, Supporting Information) and TV recovery (cf. Figure S16, Supporting Information; Figure 4) are very similar between 10 MeV proton irradiated cells and 7 MeV proton irradiated cells. This is because both 7 and 10 MeV protons travel through the entire perovskite cell with negligible implanted protons within the cell as shown in Figure S17a (Supporting Information). In fact, SRIM simulated atomic displacements by 10 MeV are slightly lower than (but in the same order of magnitude to) those by 7 MeV (Figure S17b, Supporting Information). This explains the slightly better evolution of PCEs of 10 MeV proton irradiated and post-TV PSCs compared to the 7 MeV proton irradiated cells (Figure S17c, Supporting Information).

For the 1 MeV proton irradiated cells, while radiation-damage is negligible as expected due to the shielding by the 175 µm sapphire substrate (Figures S15c and S18, Supporting Information), TV had an detrimental effect on PTAA(TPFB):Spiro(LiTFSI) cells that are not affected by radiation (Figures S15d,b and S6b, Supporting Information).

TV also caused degradation to nonirradiated PTAA(LiTFSI) and PTAA(LiTFSI):C8BTBT(LiTFSI)) cells (Figure S7b, Supporting Information) but not to PTAA(TPFB) and PTAA(TPFB):C8BTBT(TPFB) cells (Figure S6b, Supporting Information) or even PTAA(TPFB):Spiro(TPFB) cells (Figure S7b, Supporting Information). These findings suggest that it is the presence of the dopant LiTFSI rather than the presence of Spiro-OMeTAD (provided that is LiTFSI-free) that made the cells susceptible to thermal-vacuum-induced degradation and such degradation only occurred when the anneal was conducted in vacuum and not in ambient (Figure S19, Supporting Information). This may be due to the less than perfect encapsulation that fails to suppress outgassing,[39,47] that is more prominent during TV. While developing more stringent encapsulation scheme as part of future work will be useful for space cells, the elimination of HTM dopant LiTFSI will even be more effective which eliminates i) thermal-vacuum-induced degradation and ii) radiation-induced fluorine diffusion allowing cells, or more specifically the surface of the perovskite absorber, to recover by TV.

3. Conclusion

In conclusion, this is the first study on the relative radiation hardness of three different types of HTMs with two types of HTM dopants for PSCs. PSCs were subjected to irradiation with a scanned pencil beam of 7 MeV protons to achieve three different accumulated fluences of 10^{11}, 10^{12}, and 10^{13} protons cm^{-2}. The cells used in this work have much higher power to weight

ratios compared to proton-radiation-tested PSCs previously reported. These cells were fabricated on sub-millimeter sapphire superstrates that are radiation-resistant in the interest of space applications. Results showed the importance of the type of HTMs and their dopants used affecting cells' radiation hardness. Appropriate choice reduces the extent of radiation damage but also allows cells to "self-heal" via TV treatment recover their PCEs. TAS, DLTS and temperature-dependent V_{OC} measurements were carried out on cells with different HTM-dopant combinations revealing the different defect behaviors with some irreversible and some reversible by thermal anneal. This is the first time that TAS and DLTS were used to analyze defects in proton-irradiated and thermal-vacuum-recovered perovskite cells. Insights generated will contribute to efforts in developing low-cost light-weight solar cells for space application.

4. Experimental Section

Details can be found in the Supporting Information.

Supporting Information

Supporting Information is available from the Wiley Online Library or from the author.

Acknowledgements

S.T. and C.L. are supported by the John Hooke Chair of Nanoscience Postgraduate Research Scholarship. S.T. is also supported by the CSIRO postgraduate research top-up scholarship. J.B., J.Z., and M.A.M. are supported by the Australian Government through the Australian Renewable Energy Agency (ARENA) via projects 2020 RND001 and 2020 RND003, respectively. A.H.-B. acknowledges the support by the Australian Research Council (ARC) via Future Fellowship (FT210100210). G.L. acknowledges the support by the ARC Centre of Excellence in Exciton Science (CE170100026) and A.H.-B. acknowledges the Centre of Excellence Associate Investigator Support Fund for the DLTS infrastructure. G.J.W. wishes to thank the CSIRO Research Office and the Energy Technologies Program for project funding, postgraduate scholarships, and Fellowship support. The authors also acknowledge the financial support from the Australian Government for the operation of the ANTARES microprobe facility for proton irradiation at the ANSTO Centre for Accelerator Science through the National Collaborative Research Infrastructure Strategy (NCRIS). Finally, the authors acknowledge the scientific and technical assistance provided by the Research and Prototype Foundry (RPF) and Sydney Analytical which part of the Core Research Facility at the University of Sydney. RPF is part of the Australian National Fabrication Facility.

Open access publishing facilitated by The University of Sydney, as part of the Wiley - The University of Sydney agreement via the Council of Australian University Librarians.

Conflict of Interest

The authors declare no conflict of interest.

Data Availability Statement

The data that support the findings of this study are available from the corresponding author upon reasonable request.

Keywords

hole transport materials, perovskite solar cells, proton irradiation, space solar cells, thermal vacuum recovery

Received: February 16, 2023
Revised: April 14, 2023
Published online: May 22, 2023

[1] P. Iles, *Sol. Energy Mater. Sol. Cells* **2001**, *68*, 1.
[2] H. Jones, presented at *48th Int. Conf. on Environmental Systems*, Albuquerque, New Mexico **2018**.
[3] W. W. Cobb, *How SpaceX Lowered Costs and Reduced Barriers to Space*, The Conversation, Canberra, Australia **2019**.
[4] A. R. Kirmani, B. K. Durant, J. Grandidier, N. M. Haegel, M. D. Kelzenberg, Y. M. Lao, M. D. Mcgehee, L. Mcmillon-Brown, D. P. Ostrowski, T. J. Peshek, B. Rout, I. R. Sellers, M. Steger, D. Walker, D. M. Wilt, K. T. Vansant, J. M. Luther, *Joule* **2022**, *6*, 1015.
[5] M. T. Hoang, Y. Yang, B. Tuten, H. Wang, *J. Phys. Chem. Lett.* **2022**, *13*, 2908.
[6] Y. Tu, J. Wu, G. Xu, X. Yang, R. Cai, Q. Gong, R. Zhu, W. Huang, *Adv. Mater.* **2021**, *33*, 2006545.
[7] K. A. Horowitz, T. W. Remo, B. Smith, A. J. Ptak, *A Techno-Economic Analysis and Cost Reduction Roadmap for III–V Solar Cells*, National Renewable Energy Lab (NREL), Golden, CO **2018**.
[8] N. L. Chang, A. W. Yi Ho-Baillie, P. A. Basore, T. L. Young, R. Evans, R. J. Egan, *Prog. Photovoltaics* **2017**, *25*, 390.
[9] N. L. Chang, A. W. Y.i Ho-Baillie, D. Vak, M. Gao, M. A. Green, R. J. Egan, *Sol. Energy Mater. Sol. Cells* **2018**, *174*, 314.
[10] N. L. Chang, J. Zheng, Y. Wu, H. Shen, F. Qi, K. Catchpole, A. Ho-Baillie, R. J. Egan, *Prog. Photovoltaics* **2021**, *29*, 401.
[11] J. Barbé, D. Hughes, Z. Wei, A. Pockett, H. K. H. Lee, K. C. Heasman, M. J. Carnie, T. M. Watson, W. C. Tsoi, *Sol. RRL* **2019**, *3*, 1900219.
[12] V. V. Brus, F. Lang, J. Bundesmann, S. Seidel, A. Denker, B. Rech, G. Landi, H. C. Neitzert, J. Rappich, N. H. Nickel, *Adv. Electron. Mater.* **2017**, *3*, 1600438.
[13] J. Huang, M. D. Kelzenberg, P. Espinet-González, C. Mann, D. Walker, A. Naqavi, N. Vaidya, E. Warmann, H. A. Atwater, in *2017 IEEE 44th Photovoltaic Specialist Conference (PVSC)*, (Ed: T. Anderson), IEEE, Piscataway, NJ **2017**, p. 1248, https://doi.org/10.1109/PVSC.2017.8366410.
[14] S. Kanaya, G. M. Kim, M. Ikegami, T. Miyasaka, K. Suzuki, Y.u Miyazawa, H. Toyota, K. Osonoe, T. Yamamoto, K. Hirose, *J. Phys. Chem. Lett.* **2019**, *10*, 6990.
[15] F. Lang, M. Jošt, J. Bundesmann, A. Denker, S. Albrecht, G. Landi, H.-C. Neitzert, J. Rappich, N. H. Nickel, *Energy Environ. Sci.* **2019**, *12*, 1634.
[16] F. Lang, M. Jošt, K. Frohna, E. Köhnen, A. Al-Ashouri, A. R. Bowman, T. Bertram, A. B. Morales-Vilches, D. Koushik, E. M. Tennyson, K. Galkowski, G. Landi, M. Creatore, B. Stannowski, C. A. Kaufmann, J. Bundesmann, J. Rappich, B. Rech, A. Denker, S. Albrecht, H.-C. Neitzert, N. H. Nickel, S. D. Stranks, *Joule* **2020**, *4*, 1054.
[17] F. Lang, N. H. Nickel, J. Bundesmann, S. Seidel, A. Denker, S. Albrecht, V. V. Brus, J. Rappich, B. Rech, G. Landi, H. C. Neitzert, *Adv. Mater.* **2016**, *28*, 8726.
[18] Y.u Miyazawa, M. Ikegami, H.-W. Chen, T. Ohshima, M. Imaizumi, K. Hirose, T. Miyasaka, *iScience* **2018**, *2*, 148.
[19] Y. Miyazawa, M. Ikegami, T. Miyasaka, T. Ohshima, M. Imaizumi, K. Hirose, in *2015 IEEE 42nd Photovoltaic Specialist Conference (PVSC)*, (Ed: T. Anderson), IEEE, Piscataway, NJ **2015**, p. 1.
[20] F. Lang, G. E. Eperon, K. Frohna, E. M. Tennyson, A. Al-Ashouri, G. Kourkafas, J. Bundesmann, A. Denker, K. G. West, L. C. Hirst, H.-C. Neitzert, S. D. Stranks, *Adv. Energy Mater.* **2021**, *11*, 2102246.

[21] B. Xue, L. Zhang, Z. Li, W. Jiang, Y. Liang, N. Liu, C. Pan, L. Chen, T. Wang, *Nucl. Instrum. Methods Phys. Res., Sect. B* **2022**, *526*, 29.
[22] B. K. Durant, H. Afshari, S. Singh, B. Rout, G. E. Eperon, I. R. Sellers, *ACS Energy Lett.* **2021**, *6*, 2362.
[23] W. O. Herrera Martínez, N. B. Correa Guerrero, V. A. Gómez Andrade, M. Alurralde, M. D. Perez, *Sol. Energy Mater. Sol. Cells* **2022**, *238*, 111644.
[24] D. Hughes, S. M. P. Meroni, J. Barbé, D. Raptis, H. K. H. Lee, K. C. Heasman, F. Lang, T. M. Watson, W. C. Tsoi, *Energy Technol.* **2021**, *9*, 2100928.
[25] M. Imaizumi, T. Nakamura, T. Takamoto, T. Ohshima, M. Tajima, *Prog. Photovoltaics* **2017**, *25*, 161.
[26] T. Sumita, M. Imaizumi, S. Matsuda, T. Ohshima, A. Ohi, H. Itoh, *Nucl. Instrum. Methods Phys. Res., Sect. B* **2003**, *206*, 448.
[27] Best Research-Cell Efficiency Chart, https://www.nrel.gov/pv/cell-efficiency.html (accessed: July 2022).
[28] O. Almora, D. Baran, G. C. Bazan, C. Berger, C. I. Cabrera, K. R. Catchpole, S. Erten-Ela, F. Guo, J. Hauch, A. W. Y. Ho-Baillie, T. J. Jacobsson, R. A. J. Janssen, T. Kirchartz, N. Kopidakis, Y. Li, M. A. Loi, R. R. Lunt, X. Mathew, M. D. Mcgehee, J. Min, D. B. Mitzi, M. K. Nazeeruddin, J. Nelson, A. F. Nogueira, U. W. Paetzold, N.-G. Park, B. P. Rand, U. Rau, H. J. Snaith, E. Unger, et al., *Adv. Energy Mater.* **2021**, *11*, 2102526.
[29] R. He, W. Wang, Z. Yi, F. Lang, C. Chen, J. Luo, J. Zhu, J. Thiesbrummel, S. Shah, K. Wei, Y.i Luo, C. Wang, H. Lai, H. Huang, J. Zhou, B. Zou, X. Yin, S. Ren, X. Hao, L. Wu, J. Zhang, J. Zhang, M. Stolterfoht, F. Fu, W. Tang, D. Zhao, *Nature* **2023**, https://doi.org/10.1038/s41586-023-05992-y.
[30] A. W. Y. Ho-Baillie, J. Zheng, M.d A. Mahmud, F.a-J. Ma, D. R. Mckenzie, M. A. Green, *Appl. Phys. Rev.* **2021**, *8*, 041307.
[31] S. Cakaj, *Front. Commun. Netw.* **2021**, *2*, 643095.
[32] M. Albulet, Spacex v-band non-geostationary satellite system, Tech. Rep. SAT-LOA-20161115-00118, Federal Commun. Commission, Washington, DC **2017**.
[33] A. W. Y. Ho-Baillie, H. G. J. Sullivan, T. A. Bannerman, H. P. Talathi, J. Bing, S. Tang, A. Xu, D. Bhattacharyya, I. H. Cairns, D. R. Mckenzie, *Adv. Mater. Technol.* **2022**, *7*, 2101059.
[34] C. Giori, T. Yamauchi, *Space Radiation Resistant Transparent Polymeric Materials*, IIT Research Inst, Chicago, IL **1977**.
[35] R. Hansen, J. Pascale, T. De Benedictis, P. Rentzepis, *J. Polym. Sci., Part A* **1965**, *3*, 2205.
[36] E. R. Dobrovinskaya, L. A. Lytvynov, V. Pishchik, in *Sapphire: Material, Manufacturing, Applications* (Eds: V. Pishchik, L. A. Lytvynov, E. R. Dobrovinskaya), Springer US, New York **2009**, p. 177.
[37] D. Heynderickx, B. Quaghebeur, E. Speelman, E. Daly, in *38th Aerospace Sciences Meeting and Exhibit*, American Institute of Aeronautics and Astronautics, Reston **2000**, p. 371.
[38] D. Heynderickx, B. Quaghebeur, J. Wera, E. J. Daly, H. D. R. Evans, *Space Weather* **2004**, *2*, S10S03.
[39] L. Shi, M. P. Bucknall, T. L. Young, M. Zhang, L. Hu, J. Bing, D. S. Lee, J. Kim, T. Wu, N. Takamure, D. R. McKenzie, S. Huang, M. A. Green, A. W. Y. Ho-Baillie, *Science* **2020**, *368*, eaba2412.
[40] J. Liu, W. Liu, E. Aydin, G. T. Harrison, F. H. Isikgor, X. Yang, A. S. Subbiah, S. De Wolf, *ACS Appl. Mater. Interfaces* **2020**, *12*, 23874.
[41] N. Li, S. Tao, Y. Chen, X. Niu, C. K. Onwudinanti, C. Hu, Z. Qiu, Z. Xu, G. Zheng, L. Wang, Y.u Zhang, L. Li, H. Liu, Y. Lun, J. Hong, X. Wang, Y. Liu, H. Xie, Y. Gao, Y. Bai, S. Yang, G. Brocks, Q.i Chen, H. Zhou, *Nat. Energy* **2019**, *4*, 408.
[42] L. Wang, H. Zhou, N. Li, Y.u Zhang, L. Chen, X. Ke, Z. Chen, Z. Wang, M. Sui, Y. Chen, Y. Huang, L. Li, Z. Xu, Q.i Chen, L.-D. Sun, C.-H. Yan, *J. Mater. Chem. A* **2020**, *8*, 14106.
[43] N. Li, X. Niu, L. Li, H. Wang, Z. Huang, Y.u Zhang, Y. Chen, X. Zhang, C. Zhu, H. Zai, Y. Bai, S. Ma, H. Liu, X. Liu, Z. Guo, G. Liu, R. Fan, H. Chen, J. Wang, Y. Lun, X. Wang, J. Hong, H. Xie, D. S. Jakob, X. G. Xu, Q.i Chen, H. Zhou, *Science* **2021**, *373*, 561.
[44] X. Lian, J. Chen, Y. Zhang, G. Wu, H. Chen, *Chin. J. Chem.* **2019**, *37*, 1239.
[45] I. C. Kaya, R. Ozdemir, H. Usta, S. Sonmezoglu, *J. Mater. Chem. A* **2022**, *10*, 12464.
[46] R. Zhao, L. Xie, R. Zhuang, T. Wu, R. Zhao, L. Wang, L. Sun, Y. Hua, *ACS Energy Lett.* **2021**, *6*, 4209.
[47] J. Kim, N. Park, J. S. Yun, S. Huang, M. A. Green, A. W. Y. Ho-Baillie, *Sol. Energy Mater. Sol. Cells* **2017**, *162*, 41.
[48] P. Raval, M. Dhennin, H. Vezin, T. Pawlak, P. Roussel, T.-Q. Nguyen, G. N. Manjunatha Reddy, *Electrochim. Acta* **2022**, *424*, 140602.
[49] S. Tang, S. Huang, G. J. Wilson, A. Ho-Baillie, *Trends Chem.* **2020**, *2*, 638.
[50] A. D. Carter, S. Elhadj, *Modulus of Elasticity and Thermal Expansion Coefficient of ITO Film*, Lawrence Livermore National Lab (LLNL), Livermore, CA **2016**.
[51] P. Thilakan, J. Kumar, *Vacuum* **1997**, *48*, 463.
[52] J. F. Ziegler, *Nucl. Instrum. Methods Phys. Res., Sect. B* **2004**, *219-220*, 1027.
[53] A. Y. Konobeyev, U. Fischer, Y. A. Korovin, S. P. Simakov, *Nucl. Energy Technol.* **2017**, *3*, 169.
[54] R. E. Stoller, M. B. Toloczko, G. S. Was, A. G. Certain, S. Dwaraknath, F. A. Garner, *Nucl. Instrum. Methods Phys. Res., Sect. B* **2013**, *310*, 75.
[55] S. R. Messenger, E. A. Burke, R. J. Walters, J. H. Warner, G. P. Summers, *Prog. Photovoltaics* **2005**, *13*, 115.
[56] Y. Busby, A. Agresti, S. Pescetelli, A. Di Carlo, C. Noel, J.-J. Pireaux, L. Houssiau, *Mater. Today Energy* **2018**, *9*, 1.
[57] C. P. Clark, J. E. Mann, J. S. Bangsund, W.-J.u Hsu, E. S. Aydil, R. J. Holmes, *ACS Energy Lett.* **2020**, *5*, 3443.
[58] S. Cacovich, P. Dally, G. Vidon, M. Legrand, S. Gbegnon, J. Rousset, J.-B. Puel, J.-F. Guillemoles, P. Schulz, M. Bouttemy, A. Etcheberry, *ACS Appl. Mater. Interfaces* **2022**, *14*, 34228.
[59] R. F. Sekerka, *Prog. Mater. Sci.* **2004**, *49*, 511.
[60] H. Tada, J. Carter Jr, B. Anspaugh, R. Downing, *Solar Cell Radiation Handbook*, Jet Propulsion Laboratory, Pasadena, CA **1982**.